Numerical solution of the fully non-linear weakly dispersive Serre equations for flows over dry beds.

J.P.A. Pitt[a,*], C. Zoppou[a], S.G. Roberts[a]

[a]*Mathematical Sciences Institute, Australian National University, Canberra, ACT 0200, Australia*

Abstract

Keywords: Serre equations, dry bed

1. Introduction

There has recently been a push from the water wave modelling community to extend the work behind the large scale wave models built around the Shallow Water Wave Equations [1–3] into deeper water where frequency dispersion becomes significant []. There are many dispersive wave equations with different dispersive properties and various assumptions on the properties of the waves [4]. The Serre equations is one particular dispersive wave equation that has a number of desirable properties; it is fully non-linear so that no assumption is made on the relative size of the wave and secondly its dispersion relation well approximates the dispersion relation given by the linear theory for water waves [5].

For these reasons the Serre equations have been a particular focus with many developed numerical methods for the one-dimensional case [6–12]. The capabilities of these methods has been well tested for the case of completely wet horizontal beds, as this is the only scenario that currently has analytic solutions. For the case of inundation of varying bathymetry these methods remain largely untested. Although some methods [9, 10] have been compared to experimental results of inundation events. However, the lack of convergence results for this situation is a significant issue.

In this paper we describe a Finite Element Volume Method (FEVM) that is well balanced and can handle dry beds. We demonstrate that it is well-balanced using the lake at rest analytic solution and demonstrate is dry bed handling capabilities using convergence results for forced solutions and the experimental results of Synolakis [13]. These results provide a more thorough analysis of the method in the presence of dry beds than has been given previously in the literature [9, 10].

*Corresponding author

Email addresses: jordan.pitt@anu.edu.au (J.P.A. Pitt), christopher.zoppou@anu.edu.au (C. Zoppou), stephen.roberts@anu.edu.au (S.G. Roberts)

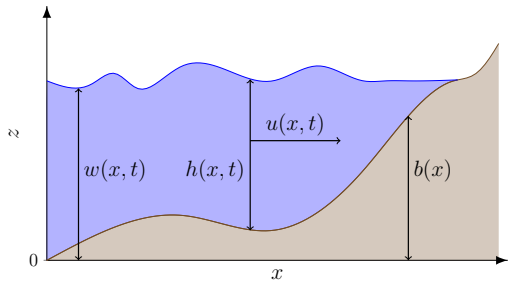

Figure 1: Diagram demonstrating a free surface flow ( ) over a bed ( ) where $w(x,t)$ is the absolute location of the free surface, $h(x,t)$ is the height of a column of fluid, $u(x,t)$ is the horizontal velocity of a column of fluid and $b(x)$ is the stationary bed profile.

2. Serre Equations

The Serre equations [14] are a system of partial differential equations that describe the free-surface waves of fluids whose motion is dominated by gravitational forces. They are a shallow-water approximation to the Euler equations [15]. The primitive variables of the Serre equations are the height of the free-surface $h(x,t)$ above the bed $b(x)$ and the average horizontal velocity over the depth of water $u(x,t)$. These variables are shown in Figure 1. Combining the bed location and the height of the free-surface gives the absolute location of the free surface $w(x,t) = h(x,t) + b(x)$.

The Serre equations can be written in conservation law form with a source term [11] like so

$$\frac{\partial h}{\partial t} + \frac{\partial (uh)}{\partial x} = 0, \tag{1a}$$

$$\begin{aligned} &\frac{\partial G}{\partial t} + \frac{\partial}{\partial x}\left(uG + \frac{gh^2}{2} - \frac{2}{3}h^3\left[\frac{\partial u}{\partial x}\right]^2 + h^2 u \frac{\partial u}{\partial x}\frac{\partial b}{\partial x}\right) \\ &\qquad + \underbrace{\frac{1}{2}h^2 u \frac{\partial u}{\partial x}\frac{\partial^2 b}{\partial x^2} - hu^2 \frac{\partial b}{\partial x}\frac{\partial^2 b}{\partial x^2} + gh\frac{\partial b}{\partial x}}_{\text{source term}} = 0 \end{aligned} \tag{1b}$$

with the conserved quantity

$$G = uh\left(1 + \frac{\partial h}{\partial x}\frac{\partial b}{\partial x} + \frac{1}{2}h\frac{\partial^2 b}{\partial x^2} + \left[\frac{\partial b}{\partial x}\right]^2\right) - \frac{\partial}{\partial x}\left(\frac{1}{3}h^3\frac{\partial u}{\partial x}\right). \tag{2}$$

2.1. Conservation Properties

Since the Serre equations can be written in conservation law form for h and G these quantities should be conserved in a closed system. Where conservation of a quantity q means that the total amount of a generic quantity q in a system occurring on the interval $[a,b]$ at time t

$$C_q(t) = \int_a^b q(x,t)\,dx$$

is constant for all t. Additionally, the Serre equations conserve the momentum uh and the energy

$$\mathcal{H}(x,t) = \frac{1}{2}\left(gh\left(h+2b\right) + hu^2 + \frac{h^3}{3}\left[\frac{\partial u}{\partial x}\right]^2 + u^2 h\left[\frac{\partial b}{\partial x}\right]^2 - uh^2\frac{\partial u}{\partial x}\frac{\partial b}{\partial x}\right).$$

The conservation of uh is a result of integrating the Serre equations in their non-conservative form [11]. While the conservation of the energy $\mathcal{H}(x,t)$ is given by the derivation of the the Green-Naghdi equations [16] which are equivalent to the Serre equations for one-dimensional flows. Indeed $\mathcal{H}$ is a sum of the gravitational and kinetic energy throughout the depth of water.

3. Method

To numerically approximate the Serre equations in conservation law form (1) the domain is partitioned into m cells $\left[x_{j-1/2}, x_{j+1/2}\right]$ of uniform length Δx. Our method begins given the location of the bed at the midpoints x_j and all the cell average values $\overline{h}_j$ and $\overline{G}_j$ at time t^n.

We reconstruct h, G and b at various points inside the cells from their given values. The reconstructed values are then used with a Finite Element Method (FEM) to solve (2) for u at various points inside the cells. We then employ a Finite Volume Method with a Source Term approximation to solve (1) obtaining a temporally first-order forward Euler time-step. Combining two first-order forward Euler steps using the second-order Strong Stability Preserving (SSP) Runge-Kutta method [17] we obtain the desired second-order accurate method. We now provide the details for all these constituent parts and the modifications to allow for dry beds.

3.1. Reconstruction

We reconstruct h, w and G with piecewise linear functions over a cell from neighbouring cell averages. While b is reconstructed from neighbouring cell midpoint values with a cubic over the cell to ensure that our approximation to $\partial^2 b/\partial x^2$ is second-order accurate. Furthermore, following the method of Audusse et al. [18] applied to the Serre equations [19] we produce an additional reconstruction $\ddot{h}$ for h from the reconstructions of w and b.

3.1.1. h,w and G

Since h, w and G use the same reconstruction operators we demonstrate them for a general quantity q. We reconstruct the values of q at $x_{j-1/2}$, x_j and $x_{j+1/2}$ from the cell averages $\overline{q}_j$ using the generalised minmod limiter [20]

$$q^+_{j-1/2} = \overline{q}_j - \frac{\Delta x}{2}d_j, \qquad q_j = \overline{q}_j, \qquad q^-_{j+1/2} = \overline{q}_j + \frac{\Delta x}{2}d_j \tag{3a}$$

where

$$d_j = \text{minmod}\left(\theta\frac{\overline{q}_j - \overline{q}_{j-1}}{\Delta x}, \frac{\overline{q}_{j+1} - \overline{q}_{j-1}}{2\Delta x}, \theta\frac{\overline{q}_{j+1} - \overline{q}_j}{\Delta x}\right) \tag{4}$$

with $\theta \in [1,2]$.

3.1.2. Bed Profile

The reconstruction cubic for b over the j^{th} cell is

$$C_j(x) = c_0\left(x - x_j\right)^3 + c_1\left(x - x_j\right)^2 + c_2\left(x - x_j\right) + c_3.$$

For a uniform mesh size the cubic has the coefficients

$$c_0 = \frac{-b_{j-2} + 2b_{j-1} - 2b_{j+1} + b_{j+2}}{12\Delta x^3}, \qquad c_1 = \frac{b_{j-2} - b_{j-1} - b_{j+1} + b_{j+2}}{6\Delta x^2},$$

$$c_2 = \frac{b_{j-2} - 8b_{j-1} + 8b_{j+1} - b_{j+2}}{12\Delta x}, \qquad c_3 = \frac{-b_{j-2} + 4b_{j-1} + 4b_{j+1} - b_{j+2}}{6}.$$

To force the continuous bed profile required by the weak form of (2) we average the two reconstructions at the cell edges $x_{j-1/2}$ and $x_{j+1/2}$ from the adjacent cells. Therefore, our reconstruction of the bed profile in the j^{th} cell is the cubic which takes these values

$$b_{j\pm1/2} = \frac{1}{2}\left(C_j(x_{j\pm1/2}) + C_{j\pm1}(x_{j\pm1/2})\right), \qquad b_{j\pm1/6} = C_j(x_{j\pm1/6}) \tag{5a}$$

3.1.3. Well Balanced $\ddot{h}$ Reconstruction

To produce the additional reconstruction $\ddot{h}$ which is also second-order accurate for the cell edge values we first calculate

$$\dot{b}^-_{j+1/2} = w^-_{j+1/2} - h^-_{j+1/2}, \qquad \dot{b}^+_{j+1/2} = w^+_{j+1/2} - h^+_{j+1/2}. \tag{6}$$

Find the maximum

$$\ddot{b}_{j+1/2} = \max\left\{\dot{b}^-_{j+1/2}, \dot{b}^+_{j+1/2}\right\}$$

then the reconstruction $\ddot{h}$ at the cell edges is given by

$$\ddot{h}^-_{j+1/2} = \max\left\{0, w^-_{j+1/2} - \ddot{b}_{j+1/2}\right\}, \qquad \ddot{h}^+_{j+1/2} = \max\left\{0, w^+_{j+1/2} - \ddot{b}_{j+1/2}\right\}. \tag{7}$$

3.2. Velocity Solve using a Finite Element Method

In the FEVM we solve for the primitive variable u given h, G and b using a FEM for (2). For the FEM we begin with the weak form of (2) using a test function v over the spatial domain Ω which is

$$\int_\Omega Gv\, dx = \int_\Omega uh\left(1 + \frac{\partial h}{\partial x}\frac{\partial b}{\partial x} + \frac{1}{2}h\frac{\partial^2 b}{\partial x^2} + \left[\frac{\partial b}{\partial x}\right]^2\right)v - \frac{\partial}{\partial x}\left(\frac{1}{3}h^3\frac{\partial u}{\partial x}\right)v\, dx.$$

Integrating by parts with zero Dirichlet boundary conditions we get

$$\int_\Omega Gv\,dx = \int_\Omega uh\left(1+\left[\frac{\partial b}{\partial x}\right]^2\right)v\,dx + \int_\Omega \frac{1}{3}h^3\frac{\partial u}{\partial x}\frac{\partial v}{\partial x}\,dx - \int_\Omega \frac{1}{2}uh^2\frac{\partial b}{\partial x}\frac{\partial v}{\partial x}\,dx - \int_\Omega \frac{1}{2}h^2\frac{\partial b}{\partial x}\frac{\partial u}{\partial x}v\,dx. \quad (8)$$

By assuming that time is fixed so that all the functions only vary in space, this formulation implies that by ensuring that G, h, b and $\partial b/\partial x$ have finite integrals over Ω, then u and $\partial u/\partial x$ must have finite integrals as well. We require $\partial u/\partial x$ to be well defined to approximate the flux and the source terms (1) and thus have finite integrals. So we will assume that for each time t that h and G are square integrable functions and b is in the Sobolev space $\mathbb{W}^{1,2}(\Omega)$ where b and its first weak derivative are square integrable functions so that u is also a member of $\mathbb{W}^{1,2}(\Omega)$.

We simplify (8) by performing the integration over the cells and then summing the integrals together to get the equation for the entire domain

$$\sum_{j=1}^{m}\left(\int_{x_{j-1/2}}^{x_{j+1/2}}\left[\left(uh\left(1+\left[\frac{\partial b}{\partial x}\right]^2\right)-\frac{1}{2}h^2\frac{\partial b}{\partial x}\frac{\partial u}{\partial x}-G\right)v + \left(\frac{1}{3}h^3\frac{\partial u}{\partial x}-\frac{1}{2}uh^2\frac{\partial b}{\partial x}\right)\frac{\partial v}{\partial x}\right]dx\right)=0 \quad (9)$$

which holds for all test functions v. The next step is to replace the functions for h, G, b, v and u with their corresponding basis function approximations.

For h and G we use the basis functions ψ which are linear inside a cell and zero elsewhere, resulting in approximations that are in the appropriate function space. For u and v we use the basis functions ϕ which are quadratic inside the cell and continuous across the cell edges so that our approximations are in $\mathbb{W}^{1,2}(\Omega)$. The basis functions of u must be quadratics to allow for a second-order approximation to $\partial u/\partial x$. Finally, for b the basis functions γ are used, they are cubic inside the cell and continuous across the cell edges so that our approximation to b is in the appropriate function space. Cubics are used for b as we require a second-order approximation to $\partial^2 b/\partial x^2$. Examples of the basis functions ψ, ϕ and γ for the j^{th} cell are given in Figure 2, from which their equations can be straightforwardly derived.

The basis functions approximation to h and G in our FEM written for a generic quantity q is

$$q = \sum_{j=1}^{m}\left(q^+_{j-1/2}\psi^+_{j-1/2} + q^-_{j+1/2}\psi^-_{j+1/2}\right) \quad (10a)$$

while for u we have

$$u = u_{1/2}\phi_{1/2} + \sum_{j=1}^{m}\left(u_j\phi_j + u_{j+1/2}\phi_{j+1/2}\right) \quad (10b)$$

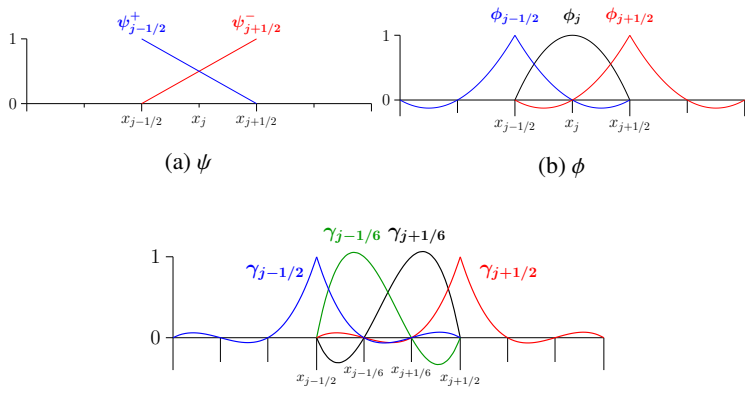

(a) ψ (b) ϕ

(c) γ

Figure 2: Support of the basis functions ψ, ϕ and γ which are non-zero over the j^{th} cell.

and finally b is

$$b = b_{1/2}\gamma_{1/2} + \sum_{j=1}^{m}\left(b_{j-1/6}\gamma_{j-1/6} + b_{j+1/6}\gamma_{j+1/6} + b_{j+1/2}\gamma_{j+1/2}\right). \tag{10c}$$

Substituting all the functions in (9) with their corresponding basis function approximations (10) the integral equation becomes a matrix equation. Assembling these matrices we get

$$\mathbf{A}\hat{\boldsymbol{u}} = \boldsymbol{g}. \tag{11}$$

Where $\mathbf{A}$ is the stiffness matrix given by the all the integrals that contain u, $\boldsymbol{u}$ is the vector containing the cell edge and midpoint values of u and $\boldsymbol{g}$ is given by the integral of Gv. This is a penta-diagonal matrix equation which can be solved by direct banded matrix solution techniques such as those of Press et al. [21] to obtain

$$\hat{\boldsymbol{u}} = \mathbf{A}^{-1}\boldsymbol{g} \tag{12}$$

as desired.

3.3. Flux Approximation

We use the method of Kurganov et al. [22] to calculate the flux across a cell interface. This method was employed because it can handle discontinuities across the cell boundary and only requires an estimate of the maximum and minimum wave speeds, which are known for the Serre equations [11].

Only the calculation of the flux term $F_{j+1/2}$ is demonstrated as the process to calculate the flux term $F_{j-1/2}$ is identical but with different cells. For a general quantity q the approximation of the flux term given by Kurganov et al. [22] is

$$F_{j+\frac{1}{2}} = \frac{a^+_{j+\frac{1}{2}} f\left(q^-_{j+\frac{1}{2}}\right) - a^-_{j+\frac{1}{2}} f\left(q^+_{j+\frac{1}{2}}\right)}{a^+_{j+\frac{1}{2}} - a^-_{j+\frac{1}{2}}} + \frac{a^+_{j+\frac{1}{2}} a^-_{j+\frac{1}{2}}}{a^+_{j+\frac{1}{2}} - a^-_{j+\frac{1}{2}}}\left(q^+_{j+\frac{1}{2}} - q^-_{j+\frac{1}{2}}\right) \tag{13}$$

where $a^+_{j+\frac{1}{2}}$ and $a^-_{j+\frac{1}{2}}$ are given by bounds on the wave speed. Applying the wave speed bounds [11] we obtain

$$a^-_{j+\frac{1}{2}} = \min\left\{0\ ,\ u^-_{j+1/2} - \sqrt{g\ddot{h}^-_{j+1/2}}\ ,\ u^+_{j+1/2} - \sqrt{g\ddot{h}^+_{j+1/2}}\right\}, \tag{14}$$

$$a^+_{j+\frac{1}{2}} = \max\left\{0\ ,\ u^-_{j+1/2} + \sqrt{g\ddot{h}^-_{j+1/2}}\ ,\ u^+_{j+1/2} + \sqrt{g\ddot{h}^+_{j+1/2}}\right\}. \tag{15}$$

Note that the reconstructed values $\ddot{h}^+_{j+1/2}$ and $\ddot{h}^-_{j+1/2}$ from (7) are used in the flux approximations [18].

The flux functions $f(q^-_{j+\frac{1}{2}})$ and $f(q^+_{j+\frac{1}{2}})$ across the cell edge $x_{j+1/2}$ are evaluated using the reconstructed values $q^-_{j+\frac{1}{2}}$ from the j^{th} cell and $q^+_{j+\frac{1}{2}}$ from the $(j+1)^{th}$ cell. From the continuity equation (1a) we have

$$f\left(h^\pm_{j+\frac{1}{2}}\right) = u^\pm_{j+1/2}\ddot{h}^\pm_{j+1/2}.$$

For the evolution of G equation (1b) we have

$$\begin{aligned} f\left(G^\pm_{j+\frac{1}{2}}\right) = u^\pm_{j+1/2}G^\pm_{j+1/2} + \frac{g}{2}\left(\ddot{h}^\pm_{j+1/2}\right)^2 - \frac{2}{3}\left(\ddot{h}^\pm_{j+1/2}\right)^3\left[\left(\frac{\partial u}{\partial x}\right)^\pm_{j+1/2}\right]^2 \\ + \left(\ddot{h}^\pm_{j+1/2}\right)^2 u^\pm_{j+1/2}\left(\frac{\partial u}{\partial x}\right)^\pm_{j+1/2}\left(\frac{\partial b}{\partial x}\right)^\pm_{j+1/2}. \end{aligned} \tag{16}$$

The quantities $\ddot{h}^+_{j-1/2}$, $\ddot{h}^-_{j+1/2}$, $G^+_{j-1/2}$ and $G^-_{j+1/2}$ were calculated during the reconstruction and the FEM provided $u^\pm_{j+1/2} = u_{j+1/2}$ as u is continuous across the cell boundaries. To calculate the derivatives $(\partial u/\partial x)^\pm_{j+1/2}$ and $(\partial b/\partial x)^\pm_{j+1/2}$ we use the reconstruction polynomials $P^u_j(x)$ and $P^b_j(x)$ for u and b respectively. These reconstruction polynomials pass through the values of u and b given over the j^{th} cell and so for $P^u_j(x)$ we obtain the coefficients

$$p^u_0 = \frac{u_{j-1/2} - 2u_j + u_{j+1/2}}{2\Delta x^2}, \qquad p^u_1 = \frac{-u_{j-1/2} + u_{j+1/2}}{\Delta x},$$
$$p^u_2 = u_j.$$

while for $P^b_j(x)$ the coefficients are

$$p^b_0 = \frac{-9b_{j-1/2} + 27b_{j-1/6} - 27b_{j+1/6} + 9b_{j+1/2}}{2\Delta x^3}, \quad p^b_1 = \frac{9b_{j-1/2} - 9b_{j-1/6} - 9b_{j+1/6} + 9b_{j+1/2}}{4\Delta x^2},$$

$$p^b_2 = \frac{b_{j-1/2} - 27b_{j-1/6} + 27b_{j+1/6} - b_{j+1/2}}{8\Delta x}, \qquad p^b_3 = \frac{-b_{j-1/2} + 9b_{j-1/6} + 9b_{j+1/6} - b_{j+1/2}}{16}.$$

Taking the derivative of the polynomials $P^u_j(x)$ and $P^b_j(x)$ we get

$$\frac{\partial}{\partial x}P^u_j(x) = 2p^u_0\left(x - x_j\right) + p^u_1,$$
$$\frac{\partial}{\partial x}P^b_j(x) = 3p^b_0\left(x - x_j\right)^2 + 2p^b_1\left(x - x_j\right) + p^b_2.$$

This gives a second-order approximation to the derivative of u and b at $x_{j+1/2}$ for the j^{th} cell. The process for the $(j+1)^{th}$ cell is the same and we get

$$\left(\frac{\partial u}{\partial x}\right)^{-}_{j+1/2} = \frac{\partial}{\partial x} P^{u}_{j}(x_{j+1/2}), \qquad \left(\frac{\partial u}{\partial x}\right)^{+}_{j+1/2} = \frac{\partial}{\partial x} P^{u}_{j+1}(x_{j+1/2}), \tag{17}$$

$$\left(\frac{\partial b}{\partial x}\right)^{-}_{j+1/2} = \frac{\partial}{\partial x} P^{b}_{j}(x_{j+1/2}), \qquad \left(\frac{\partial b}{\partial x}\right)^{+}_{j+1/2} = \frac{\partial}{\partial x} P^{b}_{j+1}(x_{j+1/2}). \tag{18}$$

3.4. Source Term Approximation

To evolve the Serre equations (1), we require an approximation to the source terms contribution over the j^{th} cell between times t^n and t^{n+1} which we denote as S^n_j. Equation (1a) has no source term, therefore we only present the calculation of the source term for equation (1b).

Following the work of Audusse et al. [18] to produce a well-balanced method, we split our approximation to S^n_j into the centred source term S_{ci} and the corrective interface source terms $S^-_{j+\frac{1}{2}}$ and $S^+_{j+\frac{1}{2}}$

$$S^n_j = S^-_{j+\frac{1}{2}} + \Delta x S_{ci} + S^+_{j-\frac{1}{2}}.$$

Where S_{ci} is the naive source term approximation and $S^-_{j+\frac{1}{2}}$ and $S^+_{j+\frac{1}{2}}$ are correction terms that ensure that the flux and source term cancel for the lake at rest solution.

We calculate the centred source term using

$$S_{ci} = -\frac{1}{2}\left(h_j\right)^2 u_j \left(\frac{\partial u}{\partial x}\right)_j \left(\frac{\partial^2 b}{\partial x^2}\right)_j + h_j \left(u_j\right)^2 \left(\frac{\partial b}{\partial x}\right)_j \left(\frac{\partial^2 b}{\partial x^2}\right)_j - g h_j \left(\frac{\partial b}{\partial x}\right)_j.$$

Where we use h_j from the reconstruction process (3) and u_j from the solution of (12). To calculate the derivatives we employ our polynomial representations of u and b (18) inside a cell. However, to ensure that the terms cancel properly for a lake at rest we modify our approximation to $\partial b/\partial x$ to use $\dot{b}^-_{j+1/2}$ and $\dot{b}^+_{j+1/2}$ from (6). Therefore, the following approximations are used to calculate S_{ci}

$$\left(\frac{\partial u}{\partial x}\right)_j = \frac{\partial}{\partial x} P^{u}_{j}(x_j), \qquad \left(\frac{\partial b}{\partial x}\right)_j = \frac{\dot{b}^-_{j+1/2} - \dot{b}^+_{j-1/2}}{\Delta x}, \qquad \left(\frac{\partial^2 b}{\partial x^2}\right)_j = \frac{\partial^2}{\partial x^2} P^{b}_{j}(x_j).$$

To ensure well-balancing the corrective interface source terms

$$S^-_{j+\frac{1}{2}} = \frac{g}{2}\left(\ddot{h}^-_{j+\frac{1}{2}}\right)^2 - \frac{g}{2}\left(h^-_{j+\frac{1}{2}}\right)^2, \qquad S^+_{j-\frac{1}{2}} = \frac{g}{2}\left(h^+_{j-\frac{1}{2}}\right)^2 - \frac{g}{2}\left(\ddot{h}^+_{j-\frac{1}{2}}\right)^2$$

are also added. These corrective terms make use of $h^-_{j+\frac{1}{2}}$ and $h^+_{j+\frac{1}{2}}$ obtained from the reconstruction (3) and the other reconstructions $\ddot{h}^-_{j+\frac{1}{2}}$ and $\ddot{h}^+_{j+\frac{1}{2}}$ from (7). Combining the centred and interface source terms our approximation to the source term for G is

$$S^n_j = S^-_{j+\frac{1}{2}} + \Delta x S_{ci} + S^+_{j-\frac{1}{2}}.$$

3.5. Time-Stepping

To increase the order of accuracy in time we employ the second-order SSP Runge-Kutta method [17] which is a convex combination of first-order forward Euler time steps in the following way

$$\overline{q}_j^{(1)} = \overline{q}_j^n + \frac{\Delta t}{\Delta x}\left(F^n_{j+\frac{1}{2}} - F^n_{j-\frac{1}{2}} + S^n_j\right), \tag{19a}$$

$$\overline{q}_j^{(2)} = \overline{q}_j^{(1)} + \frac{\Delta t}{\Delta x}\left(F^{(1)}_{j+\frac{1}{2}} - F^{(1)}_{j-\frac{1}{2}} + S^{(1)}_j\right), \tag{19b}$$

$$\overline{q}_j^{n+1} = \frac{1}{2}\left(\overline{q}_j^n + \overline{q}_j^{(2)}\right). \tag{19c}$$

This results in a time stepping method that preserves the stability of the first-order method and is second-order accurate in time. Since all the spatial approximations are second-order accurate, the FEVM should be a second-order accurate solver for the Serre equations, as desired.

3.6. Dry Bed Handling

Dry beds present two issues for the FEM; when h and G are small then small errors in h and G can produce large errors in u leading to instabilities and when $h = 0$ the stiffness matrix $\mathbf{A}$ (12) becomes singular.

The issue of large errors in u when h is small also arises when solving the SWWE; due to $u = (uh)/h$ being undefined as uh and h go to zero. For the Serre equations with horizontal beds when $h \ll 1$ from (2) we have

$$G = uh + O\left(h^3\right). \tag{20}$$

Since $h \ll 1$ we neglect the $O\left(h^3\right)$ terms, and thus when h is small G is equal to the momentum uh, and the challenges posed by $h \to 0$ for the SWWE and the Serre equations are equivalent. Therefore, we can apply the dry bed handling techniques from the SWWE to the Serre equations; in particular a desingularisation transformation [23].

These desingularisation transforms act by modifying the calculation of u given h and uh to avoid the singularity as the numerator and denominator go to zero, hence their name. The simplest such transformation is

$$u = \frac{(uh)h}{h\,(h + h_{base})} \tag{21}$$

where h_{base} is some small chosen parameter. The error introduced by this transformation is smallest when h_{base} is smallest. However, as noted by Kurganov and Petrova [23] small values of h_{base} lead to large numerical errors in the calculation of u. To avoid such errors h_{base} can be made larger or following Kurganov and Petrova [23] different desingularisation transformations can be employed. For the forced solution validation we found the simpler transformation with small values of h_{base} more useful, keeping in mind that large numerical errors in u were possible for small values of h.

To adapt the calculation of u in (21) to (2) we view it as a transformation of the quantity h which is equivalent to

$$h \to h\left(\frac{h + h_{base}}{h}\right). \tag{22}$$

This transformation is ill-defined when $h = 0$ so we also add in a small term h_{tol} to the denominator. This h_{tol} also serves as our cut-off value with any cells with $\overline{h}_j < h_{tol}$ being considered dry. Therefore, our transformation for the reconstructed values of h in the finite element method is

$$h^+_{j-1/2} = h^+_{j-1/2}\left(\frac{h^+_{j-1/2} + h_{base}}{h^+_{j-1/2} + h_{tol}}\right), \qquad h^-_{j+1/2} = h^-_{j+1/2}\left(\frac{h^-_{j+1/2} + h_{base}}{h^-_{j+1/2} + h_{tol}}\right) \tag{23}$$

where on the right hand side are the reconstructed values of h from (3) and the left hand side are the values of h used to defined the basis functions of the FEM (10a). This transformation is applied to all terms in the FEM avoiding the singularity as $h \to 0$.

Even with the transform (23), the matrix $\mathbf{A}$ can become singular. To circumvent the non-singularity an LU decomposition with partial pivoting [21] was employed. Typically we set the pivot tolerance value $p_{tol} = 10^{-20}$ allowing the matrix solver to accurately invert $\mathbf{A}$ and thus solve (12) when $h = 0$.

A cell is considered dry when $\overline{h}_j \le h_{tol}$, for dry cells we set

$$\begin{aligned} h^+_{j-1/2} &= 0, & G^+_{j-1/2} &= 0, & w^+_{j-1/2} &= b_{j-1/2}, \\ h_j &= 0, & G_j &= 0, & w_j &= b_j, \\ h^-_{j+1/2} &= 0, & G^-_{j+1/2} &= 0, & w^-_{j+1/2} &= b_{j+1/2} \end{aligned}$$

and

$$\begin{aligned} u_{j-1/2} &= 0 && \text{if} && \overline{h}_{j-1} \le h_{tol}, \\ u_j &= 0, \\ u_{j+1/2} &= 0 && \text{if} && \overline{h}_{j+1} \le h_{tol} \end{aligned}$$

this drying procedure occurs after the solution of (12). In the numerical experiments the typical values used were $h_{tol} = 10^{-12}$ and $h_{base} = 10^{-8}$.

4. Validation

To validate that the numerical method is the appropriate order of accuracy, well-balanced and can handle dry-beds we used three numerical experiments. Firstly, the convergence and conservation properties of the method for the lake at rest analytic solution were measured. Secondly, we measured the convergence of the numerical method to forced solutions. Finally, we compared our numerical solutions to the experimental results of Synolakis [13].

4.1. Measures of Convergence and Conservation

We begin the validation by defining the measures of convergence and conservation for a general quantity q. The L_2 vector norm was used to measure the difference between the numerical solutions at the cell midpoints $\boldsymbol{q}^*$ and the analytic solutions at the cell midpoints $\boldsymbol{q}$ like so

$$L_2(\boldsymbol{q}, \boldsymbol{q}^*) = \begin{cases} \dfrac{\|\boldsymbol{q}^* - \boldsymbol{q}\|_2}{\|\boldsymbol{q}\|_2} & \|\boldsymbol{q}\|_2 > 0 \\ \\ \|\boldsymbol{q}^*\|_2 & \|\boldsymbol{q}\|_2 = 0. \end{cases}$$

By investigating the behaviour of $L_2(\boldsymbol{q}, \boldsymbol{q}^*)$ for numerical solutions with varying Δx we can investigate the convergence of the method.

The conservation properties of the method are studied using the conservation error C^*. The conservation error C^* compares the total amount of q in the numerical solution at the end of the simulation $C^*(\boldsymbol{q}^*)$ to the total amount of q in the initial conditions $C^*(\boldsymbol{q})$ like so

$$C^*(\boldsymbol{q}, \boldsymbol{q}^*) = \begin{cases} \dfrac{|C^*(\boldsymbol{q}^*) - C^*(\boldsymbol{q})|}{|C^*(\boldsymbol{q})|} & |C^*(\boldsymbol{q})| > 0 \\ \\ |C^*(\boldsymbol{q}^*)| & |C^*(\boldsymbol{q})| = 0. \end{cases}$$

Where the total amount of a quantity $C^*(\boldsymbol{q})$ is calculated numerically by summing the total amount of q in each cell obtained by fifth-order accurate Gaussian quadrature of a quartic interpolation of q over the cell using the midpoint values $\boldsymbol{q}$.

4.2. Lake at Rest Solution Validation

The lake at rest is a stationary analytic solution of the Serre equations where a still lake has a horizontal water surface over any bathymetry. This solution is maintained due to the balance of the hydrostatic pressure and the forcing of the bed slope. A well-balanced numerical method should accurately reproduce this lake at rest stationary solution.

To test whether this method is well-balanced we chose the following lake at rest solution

$$h(x,t) = \max\{a_0 - b(x), 0\}, \qquad b(x) = a_1 \sin(a_2 x), \tag{24a}$$

$$u(x,t) = 0, \qquad G(x,t) = 0. \tag{24b}$$

To demonstrate the capability of the method in the presence of dry and wet beds the parameter values $a_0 = 0m$, $a_1 = 1m$ and $a_2 = 2\pi/50m^{-1}$ were chosen. These parameter values result in lakes with a horizontal free surface where the stage $w(x,t) = h(x,t) + b(x) = a_0 = 0$ (24) surrounded by dry beds.

For the numerical solutions the spatial domain was $x \in [-112.5m, 87.5m]$ and the final time was $t = 10s$, with the standard gravitational acceleration $g = 9.81m/s^2$. The spatial resolution of the method was varied so that $\Delta x = 100/2^k m$ with $k \in [8, \ldots, 17]$ and the CFL condition [24] was satisfied by having $\Delta t = Cr\Delta x/\sqrt{g}$ with condition

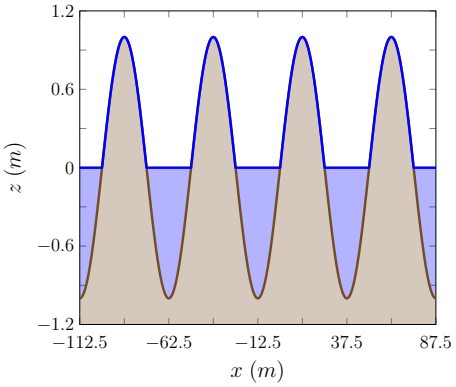

Figure 3: Numerical solution for w (■) and b (■) with $\Delta x = 100/2^{10}m$ for the lake at rest problem at $t = 10s$.

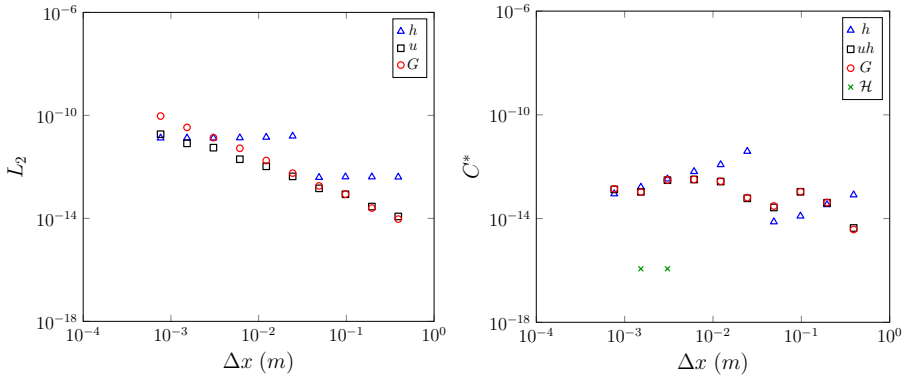

(a) Convergence (L_2)

(b) Conservation Error (C^*)

Figure 4: Convergence (h, u and G) and conservation error (h, u, G $\mathcal{H}$) against Δx for the lake at rest problem at $t = 10s$.

number $Cr = 0.5$. The standard limiting parameter $\theta = 1.2$ was used in the generalised minmod limiter (4). Dirichlet boundary conditions were used at both ends as the analytic solution is stationary.

The numerical method is assessed by using the specified lake at rest solution as initial conditions and comparing the numerical solution at $t = 10s$ to the analytic solution, which are the initial conditions.

An example numerical solution with $\Delta x = 100/2^{10}m \approx 0.0977m$ at $t = 10s$ is given in Figure 3. The numerical solution in this figure is indistinguishable from the analytic solution at this scale and so the analytic solution has been omitted.

Examination of the L_2 errors depicted in Figure 4a reveals that the method reproduced h, G and u precisely, accounting for round-off errors. For G and u their errors are increasing due to an accumulation of the round-off errors for each cell and time step; hence their increase as $\Delta x \to 0$. The errors in u produce errors in h through its flux function increasing the error in h as Δx decreases. However, since h is far larger than u

these effects have a more complicated relationship to the cell width.

The conservation error as measured by C^* for h, uh, G and $\mathcal{H}$ is given in Figure 4b. The conservation error of these conserved quantities demonstrates that all quantities are conserved within machine precision. With $\mathcal{H}$ being conserved exactly for most numerical solutions, hence its disappearance from the log-log plot. The conservation error of $\mathcal{H}$ is small for the lake at rest solution since u is very small. Hence, $\mathcal{H}$ is essentially the gravitational potential energy which since mass is well conserved is also well conserved.

These results demonstrate that the developed method has accurately reproduced the lake at rest solution and is therefore well-balanced.

4.3. Forced Solution Validation

There are currently no known analytic solution of the Serre equations for varying bathymetry with dry regions where the velocities are non-zero. To test the capability of our numerical method in this environment we must used forced solutions.

To do this we select some particular functions for all of the primitive quantities; h, u and b which we denote $h^\#$, $u^\#$ and $b^\#$ respectively. To force these functions $h^\#$, $u^\#$ and $b^\#$ to be solutions of the Serre equations (1) we add the terms S_h and S_G to obtain the forced Serre equations

$$\frac{\partial h}{\partial t} + \frac{\partial (uh)}{\partial x} + S_h = 0, \tag{25a}$$

$$\begin{aligned} &\frac{\partial G}{\partial t} + \frac{\partial}{\partial x}\left(uG + \frac{gh^2}{2} - \frac{2}{3}h^3\left[\frac{\partial u}{\partial x}\right]^2 + h^2 u \frac{\partial u}{\partial x}\frac{\partial b}{\partial x}\right) \\ &+\frac{1}{2}h^2 u \frac{\partial u}{\partial x}\frac{\partial^2 b}{\partial x^2} - hu^2 \frac{\partial b}{\partial x}\frac{\partial^2 b}{\partial x^2} + gh\frac{\partial b}{\partial x} + S_G = 0 \end{aligned} \tag{25b}$$

where

$$S_h = -\frac{\partial h^\#}{\partial t} - \frac{\partial (u^\# h^\#)}{\partial x},$$

$$S_G = -\frac{\partial G^\#}{\partial t} - \frac{\partial}{\partial x}\left(u^\# G^\# + \frac{g\left[h^\#\right]^2}{2} - \frac{2}{3}\left[h^\#\right]^3\left[\frac{\partial u^\#}{\partial x}\right]^2 + \left[h^\#\right]^2 u^\# \frac{\partial u^\#}{\partial x}\frac{\partial b^\#}{\partial x}\right)$$

$$-\frac{1}{2}\left[h^\#\right]^2 u^\# \frac{\partial u^\#}{\partial x}\frac{\partial^2 b^\#}{\partial x^2} + h^\#\left[u^\#\right]^2 \frac{\partial b^\#}{\partial x}\frac{\partial^2 b^\#}{\partial x^2} - gh^\#\frac{\partial b^\#}{\partial x}.$$

These forced Serre equations are then numerically solved by solving the Serre equations (1) with the analytic values of S_h and S_G given $h^\#$, $u^\#$ and $b^\#$. So that, the only error present in the numerical solutions of the forced Serre equations is the error produced by the numerical methods used to solve the Serre equations.

Note that since the choice of the forced solutions $h^{\#}$, $u^{\#}$ and $b^{\#}$ is arbitrary the solutions of the forced Serre equations need not be conservative or retain any properties of the underlying Serre equations.

4.3.1. Dry Bed Forced Solution Problem

To completely test the capability of the numerical method to solve the Serre equations in all circumstances the following forced solutions

$$h^{\#}(x,t) = a_0 \exp\left(-\frac{[(x-a_1 t)-a_2]^2}{2a_3}\right), \tag{26a}$$

$$u^{\#}(x,t) = a_4 \exp\left(-\frac{[(x-a_1 t)-a_2]^2}{2a_3}\right), \tag{26b}$$

$$b^{\#}(x) = a_5 \sin(a_6 x) \tag{26c}$$

for the primitive variables were chosen. These functions produce a Gaussian bump for h and u that travels at a fixed speed a_2 over a periodic bed. Thus, h and u will have constant shape and travel to the right over time. However, this is not the case for G as u and h have constant shape but the bed is periodic. With the bed terms in G (2) changing the shape of G as the Gaussian bump in h and u encounters different bed slopes.

The values $a_0 = 0.5m$, $a_1 = 2\pi/(10a_7)\, m/s$, $a_2 = -3\pi/(2a_6)\, m$, $a_3 = \pi/(16a_6)m^2$, $a_4 = 0.5m/s$, $a_5 = 1.0m$ and $a_6 = \pi/25m^{-1}$ were used. These parameter values result in a Gaussian bump in h and u that has a width much smaller than the wavelength of the bed profile and travels precisely one wavelength of the bed in $10s$. This set up tests the capability of the numerical method in the most general flow scenario with varying bathymetry, non-zero velocities and dry beds.

The domain of the numerical solutions was $x \in [-112.5m, 87.5m]$ with $t \in [0s, 10s]$. The standard gravitational acceleration $g = 9.81m/s^2$ was used. The spatial resolution of numerical methods was varied like so $\Delta x = 100/2^k m$ with $k \in [8, \ldots, 17]$. To satisfy the CFL condition [24] the temporal resolution $\Delta t = Cr\Delta x/\left(a_1 + a_4 + \sqrt{g(a_0)}\right)$ was chosen with condition number $Cr = 0.5$. The value $\theta = 1.2$ was used in the generalised minmod limiter (4) and Dirichlet boundary conditions were applied at the boundaries of the domain.

Plots of w, h, u and G are given in Figure 5 for the numerical solution with $\Delta x = 100/2^{10}m \approx 0.0977m$. The numerical solutions of w, h and G well reproduce their respective forced solutions. However, u contains large errors behind the Gaussian bump which are caused by the particular choices $h_{base} = 10^{-8}$ and $h_{tol} = 10^{-12}$ used in the desingularisation transformation applied to the FEM (12). By choosing larger values of these quantities the errors in u can be significantly damped. However, if h_{base} and h_{tol} are larger they begin to dominate the L_2 errors in h, G and uh making the convergence less obvious. This trade-off is present in all desingularisation transforms.

For our purposes the chosen desingularisation transform (23) with small h_{base} and h_{tol} values was sufficient, resulting in large observed errors in u when h is small.

The L_2 errors for h, u, uh and G in regions where $h > 10^{-3}m$ are given in Figure 6. For these regions where h is large the second-order convergence of all quantities is observed. When h is small, the second-order accuracy in the approximation of u is

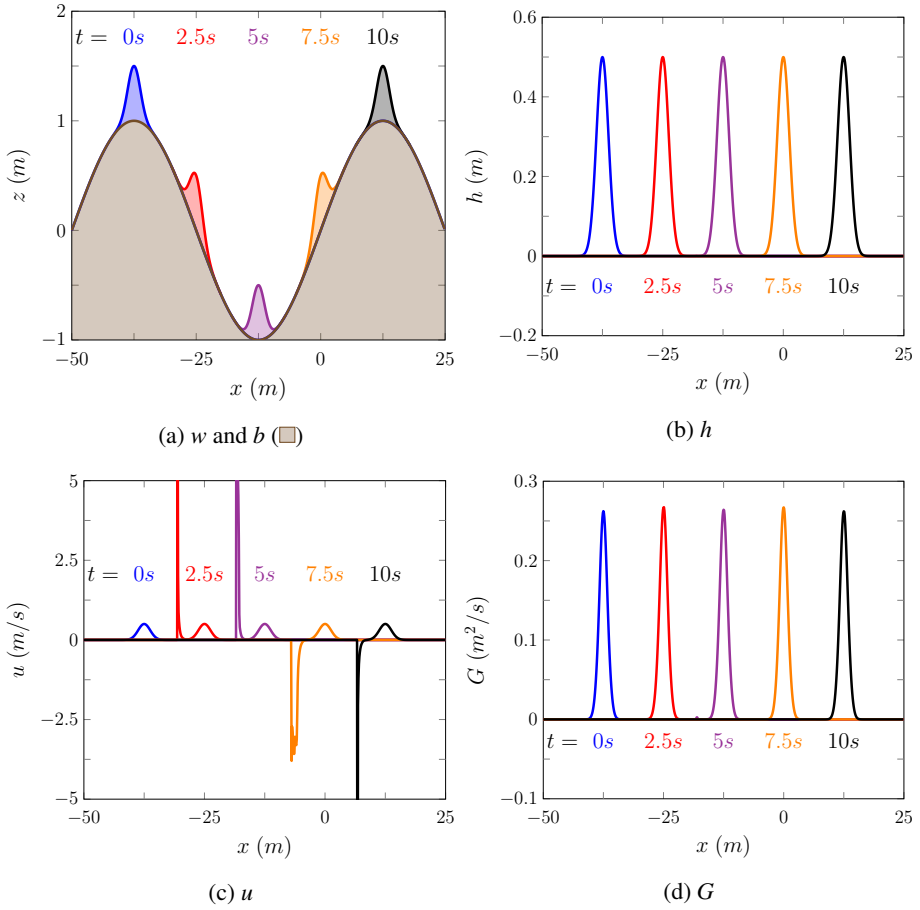

(a) w and b (□)

(b) h

(c) u

(d) G

Figure 5: Example numerical solutions for w, b, h, G with $\Delta x = 100/2^{10} m$ at various times to the dry bed forced solution problem.

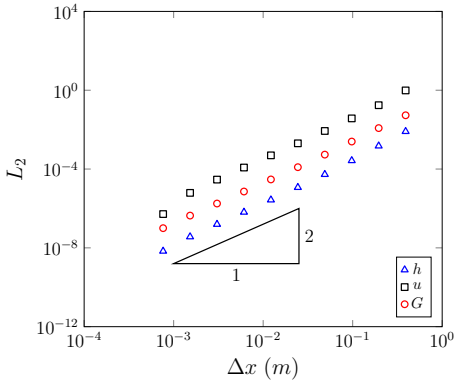

Figure 6: Convergence as measured by the L_2 in regions where $h > 10^{-3} m$ norm against Δx for h, u, and G for the dry bed forced solution problem at $t = 10s$.

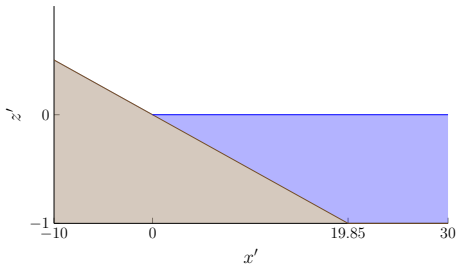

Figure 7: Diagram showing a longitudinal section of the wave tank for the run-up experiment with the water (■) and the bed (■) where the coordinates have been non-dimensionalised [13].

lost but the other quantities retain their second-order convergence as all flux and source terms depend on u multiplied by some power of h. Therefore, the large errors in u do not pollute the numerical approximation to the other quantities.

Therefore, this method retains second-order convergence for h, G and uh in the presence of dry beds, even with small h_{base} and h_{tol} values. Although, in such cases the velocity may have large errors in regions where h is small. For physical applications where large errors in u when h is small are not acceptable we recommend altering the dry bed handling of the scheme by increasing the h_{base} and h_{tol} values or altering the desingularisation transformation [23].

4.4. Run-up of a Solitary Wave

To study the run-up of incoming waves on linear beaches a series of experiments were conducted by Synolakis [13]. These experiments consisted of a number of run-up events for a wide array of breaking and non-breaking waves where snapshots of the entire water surface were taken at certain times. These experiments were all performed on the beach profile depicted in Figure 7, where all the quantities are non-dimensionalised [13]. To denote that a quantity is non-dimensionalised we use a prime; for example for a generic quantity q its non-dimensionalised version is q'. To assess the numerical method we recreated one of these experiments, which captured the run-up of a non-breaking solitary wave.

The numerical method used the non-dimensionalised quantities reported by Synolakis [13] to reproduce the experiment. The spatial domain was $x' \in [-30, 150]$ with a resolution of $\Delta x = 0.05$ and was run until $t' = 250$ with the CFL condition [24] satisfied by setting $\Delta t = 0.1\Delta x$. The spatial reconstruction used the input parameter $\theta = 1.2$ and the acceleration due to gravity $g = 1$ was chosen to match the non-dimensionalisation.

The non-dimensionalised water surface data is given at the various times in Figure 8. The error in conservation of h', $u'h'$, G' and $\mathcal{H}'$ by $t' = 250$ as measured by C^* are given in Table 1.

The numerical solutions reproduce the incoming wave properties and the maximum run-up well. The experimental wave appears to be more skewed towards the shoreline, but this shape difference has all but disappeared as the wave begins to inundate the shore. The only other noticeable difference is that the numerical solution appears to run-down further than the experimental results. The observed larger run-down is likely caused by the omission of bed friction for the Serre equations in this paper.

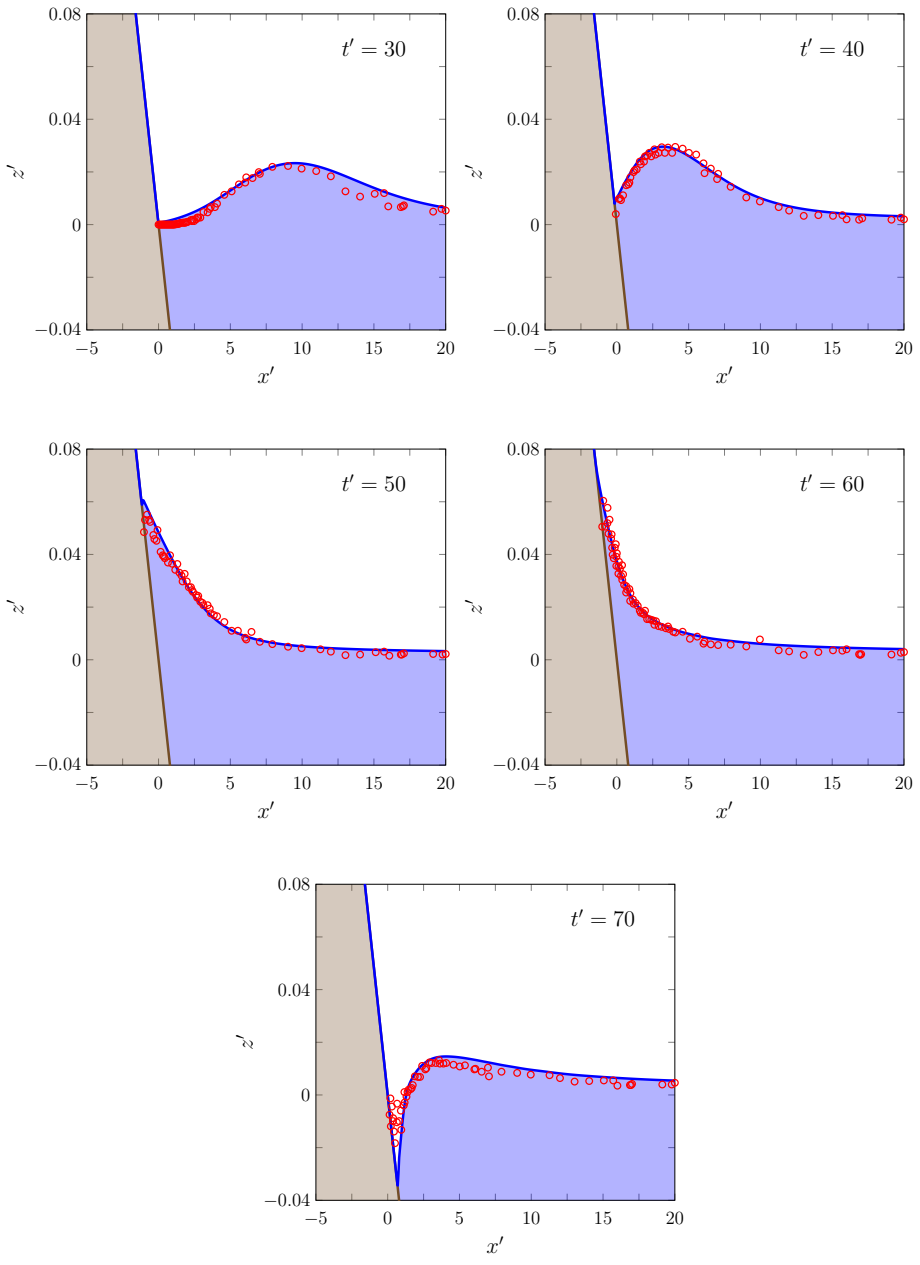

Figure 8: A comparison of the water surface profiles $w'(x', t')$ for the experiment (○) and the numerical solution (□) over the bed (□) at various times.

Quantity	$C^*\left(\boldsymbol{q}^0\right)$	$C^*\left(\boldsymbol{q}^*\right)$	$C^*\left(\boldsymbol{q}^0, \boldsymbol{q}^*\right)$
h'	240.416965344	240.416965376	1.33×10^{-10}
$u'h'$	−0.319050138516	0.318891991793	4.96×10^{-4}
G'	−0.319073723126	0.318886191223	5.88×10^{-4}
$\mathcal{H}'$	−118.389958187	−118.3900028	3.77×10^{-7}

Table 1: Initial and final ($t' = 200$) total amounts and the conservation error for the conserved quantities in the numerical solution of the run-up experiment. Here the absolute value of the total amount of uh and G are taken in the error as the wave is reflected off the beach.

Both h' and $\mathcal{H}'$ are well conserved by the method throughout the run-up and run-down of the wave, particularly h'. The total energy $\mathcal{H}'$ of the method is also well conserved, however $\mathcal{H}'$ appears to have slightly increased in the method during the run-up process due to the methods handling of the dry bed problem. During this experiment kinetic energy is converted into gravitational potential energy and then back again as the wave is reflected. By $t' = 250$ the reflection of the wave is complete and so we can see that the total amount of $u'h'$ and G' have changed signs, but accounting for this their errors are quite small. Given that kinetic energy and gravitational energy were exchanged and the handling of the dry bed, the conservation error of $u'h'$ and G' is good.

The Serre equations have reproduced the experimental result of Synolakis [13] very well. Experimentally validating the numerical methods ability to solve the Serre equations for flows over dry beds. However, the influence of dispersion during the inundation phase is not well tested here as these experimental results are also well reproduced by the SWWE [25].

5. Conclusion

A second-order FEVM was developed for the one-dimensional Serre equations with varying bathymetry. It was demonstrated to be well-balanced, second-order accurate in the presence of dry beds and compared well to experimental results. This extends the previous work in the literature by providing a convergence analysis of numerical solutions of the Serre equations in the presence of dry beds.

References

[1] S. Roberts, ANUGA, URL `https://anuga.anu.edu.au/`, 2018.

[2] X. Wang, COMCOT, URL `http://223.4.213.26/archive/tsunami/cornell/comcot.htm`, 2009.

[3] T. C. D. Team, Clawpack Documentation, URL `http://www.clawpack.org/`, 2018.

[4] D. Lannes, P. Bonneton, Derivation of Asymptotic Two-Dimensional Time-Dependent Equations for Surface Water Wave Propagation, Physics of Fluids 21 (1) (2009) 16601.

[5] E. Barthélemy, Nonlinear Shallow Water Theories for Coastal Waves, Surveys in Geophysics 25 (3) (2004) 315–337.

[6] O. Le Métayer, S. Gavrilyuk, S. Hank, A numerical scheme for the Green-Naghdi model, Journal of Computational Physics 229 (6) (2010) 2034–2045.

[7] D. Dutykh, D. Clamond, P. Milewski, D. Mitsotakis, Finite volume and pseudo-spectral schemes for the fully nonlinear 1D Serre equations, European Journal of Applied Mathematics 24 (5) (2013) 761–787.

[8] D. Mitsotakis, B. Ilan, D. Dutykh, On the Galerkin/Finite-Element Method for the Serre Equations, Journal of Scientific Computing 61 (1) (2014) 166–195.

[9] M. Li, P. Guyenne, F. Li, L. Xu, High Order Well-Balanced CDG-FE Methods For Shallow Water Waves by a Green-Naghdi Model, Journal of Computational Physics 257 (1) (2014) 169–192.

[10] A. G. Filippini, M. Kazolea, M. Ricchiuto, A Flexible Genuinely Nonlinear Approach for Nonlinear Wave Propagation, Breaking and Run-Up, Journal of Computational Physics 310 (2016) 381–417.

[11] C. Zoppou, J. Pitt, S. Roberts, Numerical Solution of the Fully Non-Linear Weakly Dispersive Serre Equations for Steep Gradient Flows, Applied Mathematical Modelling 48 (2017) 70–95.

[12] J. do Carmo, J. Ferreira, L. Pinto, G. Romanazzi, An Improved Serre Model: Efficient Simulation and comparative evaluation, Applied Mathematical Modelling 56 (2018) 404–423.

[13] C. Synolakis, The runup of solitary waves, Journal of Fluid Mechanics 185 (1987) 523–545.

[14] F. Seabra-Santos, D. Renouard, A. Temperville, Numerical and experimental study of the transformation of a solitary wave over a shelf or isolated obstacle, Journal of Fluid Mechanics 176 (1981) 117–134.

[15] L. Euler, Principes generaux du mouvement des fluides, Mémoires de l'académie des sciences de Berlin 11 (1757) 274–315.

[16] A. Green, P. Naghdi, A derivation of equations for wave propagation in water of variable depth, Journal of Fluid Mechanics 78 (2) (1976) 237–246.

[17] S. Gottlieb, C. Shu, E. Tadmor, Strong Stability-Preserving High-order Time Discretization Methods, Review, Society for Industrial and Applied Mathematics 43 (1) (2001) 89–112.

[18] E. Audusse, F. Bouchut, M. Bristeau, R. Klein, B. Perthame, A Fast and Stable Well–Balanced Scheme with Hydrostatic Reconstruction for Shallow Water Flows, Journal of Scientific Computing, Society for Industrial and Applied Mathematics 25 (6) (2004) 2050–2065.

[19] J. Pitt, A Second Order Well Balanced Hybrid Finite Volume and Finite Difference Method for the Serre Equations, Honour's thesis, Australian National University, Mathematical Sciences Institute, College of Physical and Mathematical Sciences, Australian National University, Canberra, ACT 2600, Australia, 2014.

[20] B. V. Leer, Towards the Ultimate Conservative Difference scheme. IV. A second-order sequel to Godunov's method, Journal of Computational Physics 32 (1) (1979) 101–136.

[21] W. Press, S. Teukolsky, W. Vetterling, B. Flannery, Numerical Recipes in C, Cambridge University Press, Melbourne, 2nd edn., 2002.

[22] A. Kurganov, S. Noelle, G. Petrova, Semidiscrete Central-Upwind Schemes for Hyperbolic Conservation Laws and Hamilton-Jacobi Equations, Journal of Scientific Computing, Society for Industrial and Applied Mathematics 23 (3) (2002) 707–740.

[23] A. Kurganov, G. Petrova, A second-order well-balanced positivity preserving central-upwind scheme for the Saint-Venant system, Communications in Mathematical Sciences 5 (1) (2007) 133–160.

[24] R. Courant, K. Friedrichs, H. Lewy, On the Partial Difference Equations of Mathematical Physics, IBM Journal of Research and Development 11 (2) (1967) 215–234.

[25] A. Bollermann, S. Noelle, M. Lukáčová-Medvidová, Finite volume evolution Galerkin methods for the shallow water equations with dry beds, Communications in Computational Physics 10 (2) (2011) 371–404.